A THERMAL INFRARED IMAGING STUDY OF VERY LOW-MASS, WIDE SEPARATION BROWN DWARF COMPANIONS TO UPPER SCORPIUS STARS: CONSTRAINING CIRCUMSTELLAR ENVIRONMENTS*

Vanessa Bailey[1], Philip M. Hinz[1], Thayne Currie[2], Kate Y. L. Su[1], Simone Esposito[3], John M. Hill[4], William F. Hoffmann[1], Terry Jones[5], Jihun Kim[6], Jarron Leisenring[7], Michael Meyer[7], Ruth Murray-Clay[8], Matthew J. Nelson[9], Enrico Pinna[3], Alfio Puglisi[3], George Rieke[1], Timothy Rodigas[1], Andrew Skemer[1], Michael F. Skrutskie[8], Vidhya Vaitheeswaran[1], and John C. Wilson[9]

[1] Steward Observatory, Department of Astronomy, University of Arizona
[2] Department of Astronomy and Astrophysics, University of Toronto
[3] Istituto Nazionale di Astrofisica, Osservatorio Astrofisico di Arcetri
[4] Large Binocular Telescope Observatory, University of Arizona
[5] School of Physics and Astronomy, University of Minnesota
[6] College of Optical Sciences, University of Arizona
[7] Institute for Astronomy, ETH Zurich
[8] Harvard-Smithsonian Center for Astrophysics and
[9] Department of Astronomy, University of Virginia
Accepted for publication in ApJ

ABSTRACT

We present a $3 - 5$ μm LBT/MMT adaptive optics imaging study of three Upper Scorpius stars with brown dwarf (BD) companions with very low-masses/mass ratios ($M_{BD} < 25$ M_{Jup}; $M_{BD}/M_\star \approx 1$–2%), and wide separations ($300 - 700$ AU): GSC 06214, 1RXS 1609, and HIP 78530. We combine these new thermal IR data with existing $1 - 4$ μm and 24 μm photometry to constrain the properties of the BDs and identify evidence for circumprimary/secondary disks in these unusual systems. We confirm that GSC 06214B is surrounded by a disk, further showing this disk produces a broadband IR excess due to small dust near the dust sublimation radius. An unresolved 24 μm excess in the system may be explained by the contribution from this disk. 1RXS 1609B exhibits no $3 - 4$ μm excess, nor does its primary; however, the system as a whole has a modest 24 μm excess, which may come from warm dust around the primary and/or BD. Neither object in the HIP 78530 system exhibits near-to mid-IR excesses. We additionally find that the $1 - 4$ μm colors of HIP 78530B match a spectral type of M3 $\pm$ 2, inconsistent with the M8 spectral type assigned based on its near-IR spectrum, indicating it may be a low-mass star rather than a BD. We present new upper limits on additional low-mass companions in the system (< 5 M_{Jup} beyond 175 AU). Finally, we examine the utility of circumsecondary disks as probes of the formation histories of wide BD companions, finding that the presence of a disk may disfavor BD formation near the primary with subsequent outward scattering.

Subject headings: brown dwarfs, circumstellar material, instrumentation: adaptive optics, open clusters and associations: individual (Upper Scorpius), stars: individual (GSC 06214-00210, 1RXS 160929.1-210524, and HIP 78530)

1. INTRODUCTION

Nearly all stars are born with optically thick, gas-rich, dusty accretion disks that are thought to be analogous to the early solar nebula and comprise the building blocks of planet formation. Within $5 - 10$ Myr, most of these disks disappear, having presumably converted their mass into larger, planetesimal-to-planet-mass bodies. The timescale for this process typically decreases with increasing stellar mass (Carpenter et al. 2006; Currie et al. 2009). The youngest very low-mass stars and brown dwarfs (BD) are also typically surrounded by

disks. Their disk lifetimes also tend to increase with decreasing BD mass (Luhman et al. 2008; Carpenter et al. 2009; Monin et al. 2010), though some work suggests this behavior may not be universal (Luhman et al. 2010) (hereafter L2010).

While many young, single BDs, like stars, are surrounded by optically-thick accretion disks, it is as yet unclear whether all BDs formed like stars, in particular those that are companions to stars in wide binary systems. Between $10 - 30\%$ of BDs are believed to form in binary systems (Burgasser et al. 2003; Close et al. 2003; Joergens 2008), a frequency significantly lower than that for low-mass M stars and solar-mass stars ($\gtrsim 30\%$ and $\sim 50\%$; Fischer & Marcy 1992; Janson et al. 2012b; Raghavan et al. 2010). If wide BD companions formed like other, more massive stellar binary companions, they should comprise the tail end of the binary mass function (BMF). Previous studies of the stellar BMF have found that low mass ratios ($M_B/M_A < 10\%$) are rare (e.g. Reggiani & Meyer 2011). In contrast, recent observations suggest the frequency of at least solar-type stars with very low-mass BD companions may be higher

arXiv:1302.0582v1 [astro-ph.SR] 4 Feb 2013

than expected if such objects were drawn from an extrapolation of the stellar BMF (Ireland et al. 2011; Janson et al. 2012a). Additionally, some of the lowest mass wide-separation companions have masses straddling or below the deuterium-burning limit often used to distinguish between planets and brown dwarfs (e.g. Luhman et al. 2006; Metchev & Hillenbrand 2006).

In light of these complications, several other, more planet-like, formation mechanisms have been proposed for these wide, low-mass BD companions. In these scenarios the BDs form from the primary's protoplanetary disk, either in situ or initially much closer to the primary. The first possibility is that the BDs form as part of a system of massive objects orbiting the primary and are subsequently scattered by one of these objects to their current location (e.g. Veras et al. 2009). However, a dearth of close BD companions (the so-called "brown dwarf desert") has been shown observationally and suggested theoretically (Marcy & Butler 2000; Bate 2000). Another possibility is planet-like formation in situ via direct collapse within the primary star's protoplanetary disk (e.g. Boss 2011). However, the typical stellar protoplanetary disk radius is $20 - 200~AU$, so BDs formed at separations $> 200~AU$ would require stellar hosts with unusually large disks (Andrews et al. 2009). Furthermore, the mass ratios and separations of wide BD companions are distinct from those of RV-detected planets as well as the directly-imaged planets/candidates around HR 8799, β Pic, Fomalhaut, and κ And (Marois et al. 2008a, 2010; Lagrange et al. 2010; Kalas et al. 2008; Currie et al. 2012; Carson et al. 2013), indicating that they may comprise a distinct population with a separate formation mechanism (e.g. Kratter et al. 2010).

High-contrast imaging observations of these BD companions and constraints on their disk population may clarify their formation mechanism. If wide BD companions at hundreds of AU separation form in situ as the tail end of the binary mass function (just like stellar companions), we expect that they have the same disk fraction as single BDs, since binarity at these wide separations appears to not affect circumstellar disk evolution (Jensen et al. 1996; Pascucci et al. 2008; Kraus et al. 2012). If they have a more planet-like formation mechanism, they are still likely to be born with disks. In our own Solar System, this is evidenced by the system of coplanar moons around Jupiter (Lunine & Stevenson 1982; Canup & Ward 2002). However, if these BDs form initially much closer to the primary and are scattered to their current locations, their disk masses may not be great enough to survive to the present day, as we will demonstrate. Furthermore, an intermediate-mass perturber should be present close to the primary star and may be detectable in imaging data.

The nearby Upper Scorpius OB Association (USco) provides a good testbed for these scenarios. Its youth $(5 - 10~Myr$, Preibisch et al. 2002; Pecaut et al. 2012; Song et al. 2012) and large number of members ($N \gtrsim$ 500, Preibisch et al. 2002) mean that a significant population of massive disks remains, allowing for a robust statistical sampling of the association's disk population from early to late-type stars and BDs (Carpenter et al. 2006, 2009; Luhman & Mamajek 2012). Its proximity (145 pc) provides good sensitivity at low disk and companion masses (de Zeeuw et al. 1999; Preibisch et al.

2002). About 25% of the M-type BDs in USco exhibit broadband mid-infrared excess emission from warm dust in circum(sub)stellar disks (Scholz et al. 2007; Riaz et al. 2009, 2012; Luhman & Mamajek 2012; Dawson et al. 2013). Sensitivity limits have thus far precluded similar studies of less massive L-type members.

Furthermore, USco includes three stars with recently discovered wide-separation, very low mass (ratio) BD companions: GSC 06214-00210 (GSC 06214), 1RXS 160929.1-210524 (1RXS 1609), and HIP 78530; (Ireland et al. 2011; Lafrenière et al. 2008, 2011), one of which, GSC 06214B, has been discovered to retain a hot circum(sub)stellar disk (Bowler et al. 2011). The first two systems both are K-type primaries and L-type BDs, while the third is a B-type primary and M-type BD. These three systems constitute the lowest known mass ratio binary systems in USco: $q \approx 1$–2%, which is exceedingly rare in stellar binaries, regardless of the primary star's mass (e.g. Reggiani & Meyer 2011). In fact these are among the highest mass contrast non-planetary systems found to date, populating the region of parameter space between planetary systems and stellar binaries. By probing the circum(sub)stellar environments of these and other similar systems, it may be possible to discriminate between the various suggested formation histories; here we take the first steps towards that goal.

To explore the circumstellar properties of these very low mass ratio pairs, we present and analyze new adaptive optics-resolved near/thermal IR imaging in four bands [3.1 μm, 3.3 μm, L' and M'] as well as archival unresolved Spitzer/MIPS-24 μm photometry. In each system we search for the presence of a hot circum(sub)stellar disk component around the BD, identifiable by broadband infrared excess emission in our array of resolved $1 - 5~\mu m$ data. This emission is due to small dust, with temperatures above several hundred Kelvin, located in the innermost (hot) disk where accretion is likely to be active (Tuthill et al. 2001). The MIPS-24 μm data probes the presence of warm ($T_{eff} \sim 100~K$) dust in the system, although the large beam size of these observations precludes us from determining whether warm dust emission originates from around the primary or the secondary (or both).

Our study is organized as follows. Section 2 describes our sample in more detail, our observations, and our data reduction. In Section 3, we re-examine the companions' spectral types and assess their near and mid-IR excesses using these new data. With our high-resolution adaptive optics (AO) imaging we are also able to provide constraints on the presence of additional companions in the systems. We further examine the disk properties of GSC 06214B and the nature of HIP 78530B in Section 4, discuss the utility of disks as probes of scattering histories in Section 5, and summarize our findings in Section 6.

2. SAMPLE, OBSERVATIONS AND DATA REDUCTION

2.1. *Sample*

Here we summarize the basic system properties of the three newly-identified very low-mass (ratio) BD companions that are the subject of our study:

- GSC 06214A is a 0.9 $M_\odot$ K7 star. Its membership is based on proper motion as well as on

the youth indicators: X-ray emission, Hα emission, and lithium absorption (Bowler et al. 2011, and references therein). GSC 06214B orbits at 2.20″ (320 AU) projected separation. Ireland et al. (2011) confirmed its common proper motion over a 3 yr baseline and assigned it a spectral type of L0 and a mass of 14 ± 2 M_{Jup} based on 5 Myr DUSTY models (Chabrier et al. 2000). Bowler et al. (2011) spectroscopically confirmed the object, and further suggested it is still actively accreting from a proto-planetary disk based on a 4 μm IR excess and Paβ emission.

- 1RXS 1609A is another 0.9 $M_{\odot}$ K7 star, with membership determined similarly to GSC 06214A (Lafrenière et al. 2008, and references therein). 1RXS 1609B orbits at 2.22″ (320 AU) projected separation. Lafrenière et al. (2010) measured its common proper motion over a 1 yr baseline and spectroscopically identified it as a young L4 spectral type. Unlike for GSC 06214B, the near-IR (NIR) spectrum of this object shows no sign of active accretion. At 8^{+4}_{-2} M_{Jup} (based on 5 Myr DUSTY models), this object is below the deuterium-burning limit nominally separating brown dwarfs from planets (Spiegel et al. 2011), although it has a higher mass ratio and much larger separation than directly-imaged planets such as β Picb and HR 8799bcde (Lagrange et al. 2010; Marois et al. 2008a, 2010). Thus, for simplicity we refer to this object as a BD.

- HIP 78530A is a $\sim$ 2.5 $M_{\odot}$ B9 star (Lafrenière et al. 2011, and references therein); its USco membership is based on direct parallax measurements by the Hipparcos survey (157 ± 13 pc, van Leeuwen 2007). HIP 78530B was discovered at a projected separation of 4.5″, or $\sim$ 700 AU, by Lafrenière et al. (2011). The authors confirmed its common proper motion over a 2 yr baseline and spectroscopically classified the BD as a low-surface gravity M8. They used 5 Myr DUSTY models to estimate a mass of 23 ± 3 M_{Jup}. As with 1RXS 1609B, this object's NIR spectrum shows no indication of active accretion.

These three systems (Figure 1) may probe two very different epochs in stellar evolution for the primaries and different internal structures for the companions. The B star HIP 78530A is on or near the main sequence, while the K stars 1RXS 1609A and GSC 06214A are still descending onto the main sequence. HIP 78530B is a BD whose mass is clearly above the deuterium-burning limit, while GSC 06214B is near, and 1RXS 1609B is likely below, this limit (for an assumed age of 5 Myr).

2.2. Observations

For resolved $3-5$ μm observations of each system, we used the near/thermal-infrared imaging camera, Clio, at the 6.5 m MMT and/or the Large Binocular Telescope Interferometer (LBTI) at the 8.4 m LBT (in single-sided, non-interferometric mode). A summary of these observations is presented in Table 1. At 24 μm, we used
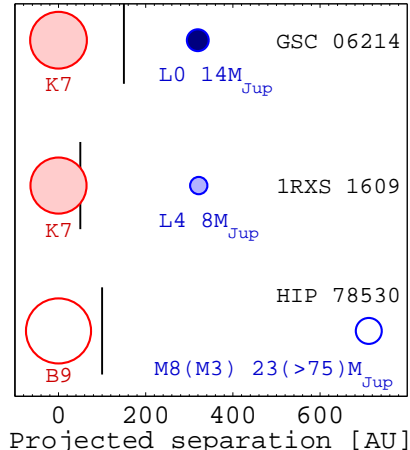

Figure 1. Schematic diagram of the three USco system properties (discussed further in Sections 3 and 4). Circle diameters are proportional to the log of the object's mass. The black line is the projected separation beyond which objects as luminous as the "B" components would have been detected in the literature or our data. Fill indicates disk properties: objects without $1-5$ μm or 24 μm excess are open circles; the dark fill of GSC 06214B signifies its $1-5$ μm excess and actively accreting disk; light shading refers to unresolved 24 μm excess in the system which may be around the primary and/or companion.

archival Spitzer/MIPS data for all three systems. Because the MIPS point-spread function (PSF) full-width half-maximum (FWHM) is $1.3 - 2.7$ times the projected separations of each companion from its host star, none of the systems are resolved at 24 μm.

2.2.1. LBT/LBTI/LMIRCam L' and M' Imaging of GSC 06214 and HIP 78530

The L and M Infrared Camera (LMIRCam) is the $3-5$ μm channel of LBTI (Hinz et al. 2008; Skrutskie et al. 2010). The field of view with an $f/15$ beam is 11″ square, with 10.7 mas pixels (calibrated Nov. 2011 by Rodigas et al. (2012)). We assume the instrument rotation angle is repeatable to 1°. Field distortion has not been measured observationally; ZEMAX models of the LMIRCam optics predict field distortions of $< 2\%$ over distances $< 5''$.

The LBT AO system employs a deformable secondary mirror in order to minimize the number of warm surfaces along the optical path. As a result, it benefits from increased sensitivity in the thermal IR (Lloyd-Hart 2000). For system details see Esposito et al. (2011) (E11). The LBTI AO hardware design is identical to that used in E11, but the calibration is independent. We corrected 200 aberration modes, rather than the 400 modes E11 used to achieve $> 80\%$ Strehl ratio (SR) in H band. At the time of these observations, the LMIRCam PSF was degraded due to residual instrumental astigmatism (which has since been mitigated). Nonetheless, because wavefront phase errors decrease with increasing wavelength, our observations approached the diffraction limit. During this run, we achieved a SR on LMIRCam of $\sim$ 80% at M' on α CrB ($R = 2.2$) at airmass $\sim$ 1. Data recorded directly from the wavefront sensor itself, not subject to the LMIRCam instrumental astigmatism, indicate the AO system was delivering $\sim$ 90% SR during these observations. The science observations were executed under more difficult conditions: low elevation

Table 1
Summary of LMIRCam and Clio observations.

Object	Date	Instrument	Filter	Wavelength Range (μm)	Integration (min)
GSC 06214	2011 May 26	LMIRCam	M'	$4.60 - 4.97$	30
	2011 Apr 22	Clio	$3.1\ \mu m$	$3.03 - 3.16$	45
	2011 Apr 22	Clio	$3.3\ \mu m$	$3.13 - 3.52$	20
1RXS 1609	2011 Apr 17	Clio	$3.1\ \mu m$	$3.03 - 3.16$	45
	2011 Apr 17	Clio	$3.3\ \mu m$	$3.13 - 3.52$	30
HIP 78530	2011 May 26	LMIRCam	L'	$3.42 - 4.12$	15

(high airmass), increased winds, and with fainter guide stars, and so were subject to poorer AO performance than the α CrB observations. Thus the sensitivities we derive in this paper are somewhat lower than those which can now be achieved with LBTI on more favorable targets (e.g. Rodigas et al. 2012; Skemer et al. 2012) or with its recently improved AO calibrations.

We observed GSC 06214 and HIP 78530 on UT 2011 May 26. During this LBTI commissioning run, only the AO system on the right LBT aperture was fully operational, so we observed in single aperture mode. The observing strategy for these, and all other LBTI observations, was Angular Differential Imaging (ADI) (Marois et al. 2006): the instrument rotation angle was fixed, and the field was allowed to rotate on the detector over the course of the observations. We used a four position nod pattern for taking image data, with nods of $1.5 - 3''$. Due to the high sky background, we were limited to very short exposures: $87\ ms$ at M' and $146\ ms$ at L'. To limit data volume, 200 individual exposures were coadded per single saved image. We obtained 30 min of M' data on GSC 06214 and 15 min of L' data on HIP 78530. The FWHM (average of major and minor axes of the astigmatic PSF) for the HIP 78530 (L') and GSC 06214 (M') images were $0.12''$ and $0.18''$, respectively.

2.2.2. *MMT/Clio 3.1 μm and 3.3 μm Narrowband Imaging of GSC 06214 and 1RXS 1609*

Clio is also a narrow-field $3-5\ \mu m$ imager (Sivanandam 2006). At the time of these observations it was installed on MMT; it is now at the Magellan Clay telescope. The MMT AO system has an architecture similar to that of LBT AO, with a deformable secondary mirror correcting 52 aberration modes (Brusa et al. 2004). In $f/15$ mode, the Clio plate scale is $29.9 \pm 0.1\ mas\ pixel^{-1}$, and the field of view of the entire array is $15'' \times 30''$ (calibrated July 2010 using the binary system HIP 88817). We assume the instrument rotation angle is repeatable to $0.1°$. Plate scale distortion has not been measured, but ZEMAX models predict distortion of $< 0.2\%$ over 5" separations.

We observed 1RXS 1609 and GSC 06214 on UT 2011 April 17 and 22, respectively. In order to decrease time lost to detector readout, we used only a subarray with a field of view of $9'' \times 30''$. Integrations were 10 coadds of $5 - 6\ s$ at $3.1\ \mu m$ and 40 coadds of $1\ s$ at $3.3\ \mu m$. The data were taken in ADI mode in a $15''$ two-position nod, with $1 - 2''$ dithers between nods. These observations suffered from moderate wind from the South that induced vibrations in the telescope and caused smearing in some of the images. The resultant FWHM ranged from $0.20'' - 0.35''$, depending on the severity of the vibrations.

On GSC 06214, we obtained approximately 45 min and 20 min of on-source integration in the $3.1\ \mu m$ and $3.3\ \mu m$ narrowband filters, respectively. On 1RXS 1609 we obtained 45 min of integration at $3.1\ \mu m$ and 30 min at $3.3\ \mu m$.

2.2.3. *Spitzer/MIPS 24 μm Imaging*

Each system had been previously observed by MIPS. 1RXS 1609 and HIP 78530 24 μm photometry are published in Carpenter et al. (2009), and we refer the reader to this publication for a description of the observations. For GSC 06214, we analyzed archival MIPS data taken as part of the Spitzer Legacy program: Gould's Belt (PID 30574, PI: L. Allen), which aimed to provide a complete census of star-forming clouds in the solar neighborhood. GSC 06214 was imaged in two AORs: 20000768 and 20001280, obtained with the fast scan rate (3 s per frame). The system was located near the end of the scan map; therefore, only 5 frames per pointing were obtained near the source position with an equivalent integration time of 15 s at 24 μm. We detected the source only at 24 μm due to the shallowness of the survey; we found no source in the corresponding 70 and 160 μm maps. Therefore, we only discuss the 24 μm result hereafter. Multiple frames were mosaicked based on the image WCS pointing information and subsampled by a factor of 2, resulting in a plate scale of $1.245''\ pixel^{-1}$.

2.3. *Image Processing*
2.3.1. *LMIRCam and Clio Data*

Custom MATLAB scripts were used for reducing the LBTI and Clio data. Background, bias, and dark subtraction were achieved by differencing images from adjacent nods. Bad pixels were flagged using a nearest-neighbors median filter and replaced with that median. In LMIRCam, each of the channels had a small time-varying bias level offset as well as variable pattern noise. We subtracted the median value of each channel to remove the offset. Then we subtracted a 2-D template of the channel read noise created from the median of all channels. For those calculations we masked out a $\sim 2''$ square region containing the source to avoid biasing the median. Finally, we aligned the images according to their position angle, rotating so North was up.

These observations did not achieve sufficient on-sky rotation to synthesize and subtract the primary's PSF, as per Marois et al. (2006). However all secondaries were sufficiently separated from their primaries ($> 2''$) that contamination from the primary was negligible. To produce the final image, we mean-combined our set of rotated images together, and $3 - 4\sigma$ outliers for each pixel in the image stack were clipped.

Aperture photometry was used to extract the differential flux between primary and secondary. None of the objects were resolved, so we used aperture radii of ~ 1 FWHM. The background was estimated using neighboring apertures of the same radius at the same separation from the host star. No aperture correction was necessary, because the same aperture radius was used for both the primary and secondary.

We next calculated sensitivity as a function of radial separation from the primary star. Residual low-spatial frequency offsets were removed by subtracting a smoothed image (Gaussian FWHM=$10\lambda/D$) from the science image. The resulting image was then smoothed with a disk the same diameter as the aperture used for photometry. The noise, σ, as a function of separation was calculated by measuring the standard deviation of 1 pixel wide annuli centered on the primary. From this we calculated the signal to noise ratios (SNR) of our detections. The uncertainty in our photometry (in magnitudes) is given by $2.5 \cdot (ln(10) \cdot SNR)^{-1}$. The noise counts as a function of radius were also converted to contrast (delta magnitudes between the primary star and the measured quantity, noise in this case) by comparing to the peak pixel value of the primary star in the smoothed image.

The primary star photometry in our filters was estimated by interpolating between published photometry in adjacent filters (i.e.: between shorter and longer wavelength photometry), because no standard stars were observed. There are no strong spectral features in K7 or B9 stars between 2 μm and 5 μm which would bias this interpolation. The 2MASS and WISE surveys recorded unresolved photometry for each system. Additionally, Carpenter et al. (2006) conducted a Spitzer IRAC survey which included 1RXS 1609 and HIP 78530. As we will show, the BD contribution to the system flux at $1 - 5$ μm is negligible, so we can treat 2MASS, WISE W1 and W2, and Spitzer IRAC photometry as measurements of the primary star only. Where available, we also used resolved photometry at additional wavelengths from previous work. The data used for interpolation are listed in Tables 2, 3, and 4.

2.3.2. *Spitzer MIPS Data*

We reduced the raw 24 μm data of GSC 06214 using the MIPS Data Analysis Tool (Gordon et al. 2005) with post-pipeline processing to improve flat fielding and remove instrumental artifacts as detailed in Engelbracht et al. (2007). We extracted the photometry using PSF fitting with the IDL-based *StarFinder* program (Diolaiti et al. 2000). The input PSF was constructed using observed stars and a smoothed STINYTIM model PSF; it has been tested to ensure the photometry results are consistent with the MIPS calibration (Engelbracht et al. 2007).

3. RESULTS AND ANALYSIS

In this section, we present photometry and analysis for each of the three binary systems. We first measure photometry for both components, from both our newly obtained high-resolution near-IR imaging and archival unresolved Spitzer 24 μm imaging. Interstellar extinction/reddening can mimic the red excess from a hot disk component; the average extinction towards USco is small

($A_V < 1$), but not negligible, and we estimate it as necessary. We re-examine the companions' spectral types and constrain their near-IR (hot dust) excesses based on their placement in color-color diagrams compared to similarly young low-mass objects. We use unresolved Spitzer 24 μm data to probe the warm dust in the system as a whole (both A and B components together). Finally, we quantify our sensitivity to additional objects in the system at intermediate separations from the primary.

3.1. *GSC 06214*
3.1.1. *Photometry and Astrometry*

The final Clio images at 3.1 μm and 3.3 μm are shown in Figure 2. At 3.1 μm we measured a contrast between "A" and "B" of 5.26 magnitudes, and at 3.3 μm we measured a contrast of 5.30 magnitudes. Using the procedure described in Section 2.3.1, we inferred the 3.1 μm and 3.3 μm magnitudes of the primary to be 9.11 ± 0.05 and 9.10 ± 0.05, respectively. The 5σ sensitivity limits for these two filters were magnitudes 15.82 and 16.14, yielding signal to noise ratios of 18 and 23 for the detections in each wavelength. From this we derive, $[3.1]_B = 14.41 \pm 0.08$ and $[3.3]_B = 14.40 \pm 0.07$ (Table 2).

We calculated a separation of $2.17\pm0.02''$ and a position angle of $175.9\pm0.1°$, consistent at the 1.5σ level with astrometry measured by Ireland et al. (2011). Because the companion was not detected in individual frames, we estimated the uncertainty by comparing the values calculated from the final images at each wavelength. Our quoted uncertainty accounts for this comparison as well as our assumed uncertainties in calibration and distortion (see Section 2.2.2).

The final LMIRCam M' image is also presented in Figure 2. The BD was detected at a contrast of 4.65 magnitudes. For the primary, we estimated $M'_A = 9.10\pm0.05$. Based on the 5σ sensitivity limit of 13.39 mag, the BD detection has $SNR = 3.6$, and therefore $M'_B = 13.75\pm0.3$. Even though this SNR is lower than that nominally adopted to identify candidate companions in high-contrast imaging data ($5-6\sigma$; Marois et al. 2008a), we also detect point sources at the same location in the 3.1 μm and 3.3 μm images, justifying a lower detection threshold. The bright spot $\sim 1''$ to the east of the primary does not appear in the more sensitive 3.1 and 3.3 μm images and is almost certainly an artifact.

The 24 μm flux density of the system is 3.3 ± 0.3 mJy (8.34 ± 0.1 mag); the error is dominated by shot noise.

3.1.2. *Extinction Estimate*

GSC 06214A did not have a published extinction value, so we performed our own estimate. We found $A_V \leq 0.6$ using the following prescription. We compared the primary's flux-calibrated optical spectrum (courtesy Bowler et al. 2011) with Pickles (1998) spectral standards (Figure 3). The observed and template spectra were normalized by their $800 - 900$ nm averages. Interstellar extinction curves with $R_V = 3.1$ (Cardelli et al. 1989) were used. Based on χ^2 fitting, both K7V with $A_V = 0$ and K5V with $A_V = 0.6$ provide acceptable fits to the data. K4V and $A_V = 0.85$ is a worse fit to both the continuum and spectral features. In order to make the most conservative estimate of the IR excess in the system, we adopt
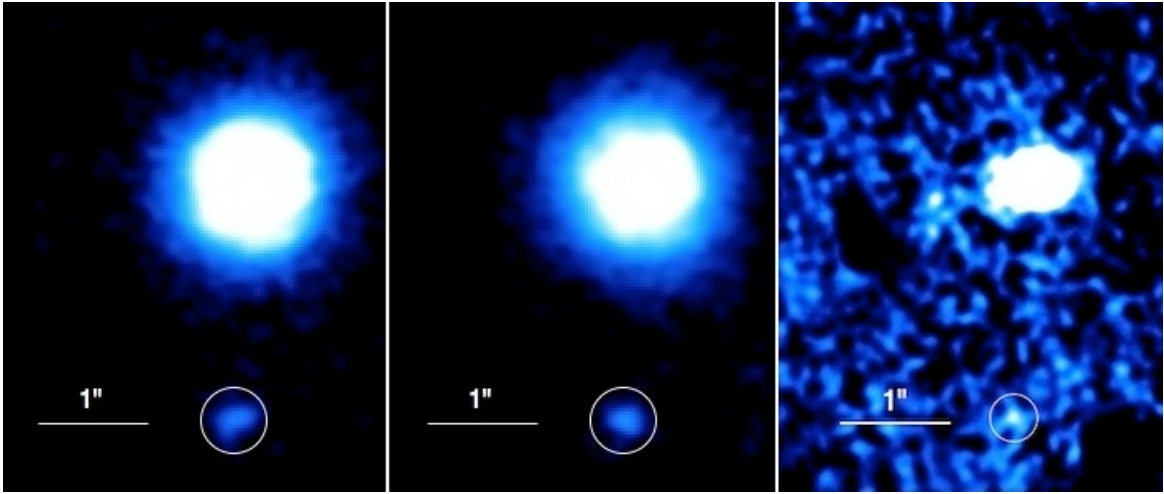
Bailey et al.

Figure 2. GSC 06214 Clio and LBTI images. *Left:* Clio 3.1 μm. *Center:* Clio 3.3 μm. *Right:* LBTI M'. The companion, circled, is $2.2''$ to the south of the primary. For display purposes, all images have been smoothed with a Gaussian kernel with FWHM=$1\lambda/D \sim 0.1''$. In the M' image, the bright spot to the left of the primary is an artifact; the dark spots to the left and bottom right are residuals from nod subtraction.

Table 2
GSC 06214-00210 system properties and
apparent photometry.

Property	GSC 06214A	GSC 06214B
Distance [pc] [a]	145 ± 20	
Spectral type [b]	K7$\pm$0.5	L0$\pm$1
Mass [b]	0.9$\pm$0.1 $M_\odot$	14$\pm$2 M_{Jup}
T_{eff} [K] [b]	4200$\pm$150	2200$\pm$100
$log(L/L_\odot)$ [b]	-0.42$\pm$0.08	-3.1$\pm$0.1
Separation [''] [c]	2.17$\pm$0.02	
PA [°] [c]	175.9$\pm$0.1	
J	9.998$\pm$0.027 [d]	16.24$\pm$0.04 [e]
H	9.342$\pm$0.024 [d]	15.55$\pm$0.04 [e]
K	9.152$\pm$0.021 [d]	14.95$\pm$0.05 [e]
3.1 μm [c]	9.11$\pm$0.05	14.41$\pm$0.08
3.3 μm [c]	9.10$\pm$0.05	14.40$\pm$0.07
3.4 μm [f]	9.083$\pm$0.022	
L' [e]	9.10$\pm$0.05	13.75$\pm$0.07
4.6 μm [f]	9.107$\pm$0.020	
M' [c]	9.10$\pm$0.05	13.75$\pm$0.3
12 μm [f]	8.964$\pm$0.032	
24 μm [c]	8.34$\pm$0.1	

[a] Mean cluster distance (de Zeeuw et al. 1999; Preibisch et al. 2002).
[b] Bowler et al. (2011).
[c] This work.
[d] 2MASS $J/H/K_S$ survey (Skrutskie et al. 2006).
[e] Ireland et al. (2011). MKO $J/H/K'/L'$.
[f] System. WISE survey (Wright et al. 2010).

the maximum allowed extinction value: $A_V = 0.6\ mag$.

3.1.3. *Spectral Classification and Evidence for a Near-IR Excess*

We placed GSC 06214 in infrared color-color diagrams, compared to several observational brown dwarf and planet samples: field brown dwarfs (Leggett et al. 2010), very young substellar objects (L2010), the young planetary-mass object 2M 1207b (Chauvin et al. 2004; Mohanty et al. 2007; Skemer et al. 2011; Barman et al. 2011), and the planets HR 8799bcd (Marois et al. 2008b, 2010; Currie et al. 2011; Galicher et al. 2011; Skemer et al. 2012). The L2010 sample of M0−L0 dwarfs was derived from dereddened observations of Taurus,
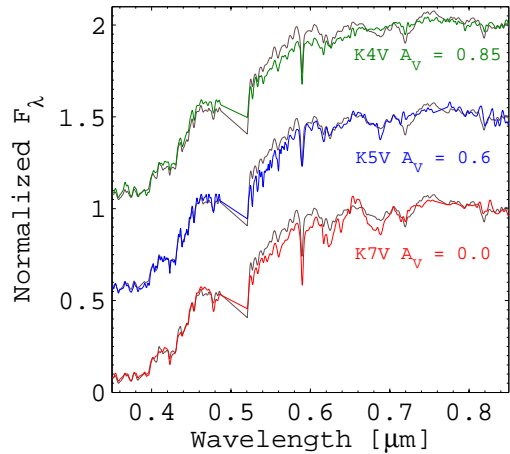

Figure 3. GSC 06214A flux vs. wavelength for best fit spectral type and extinction. F_λ is offset vertically for clarity. Gray is the stellar spectrum (Bowler et al. 2011), red is a K7V with no extinction, blue is a K5V with $A_V = 0.6\ mag$, and green is a K4V with $A_V = 0.85\ mag$. We find $A_V \leq 0.6\ mag$ for the primary.

Chameleon, and TW Hya, so it provides the most appropriate comparison sample for our similarly young brown dwarfs.

In order to conduct a homogeneous analysis, we transformed all previously published J, H, and K BD photometry to the MKO $J/H/K$ system. For 2MASS $J/H/K_S \rightarrow$ MKO $J/H/K$, we used the transformations published in Leggett et al. (2006). For MKO $K' \rightarrow K$ of stars, we used Wainscoat & Cowie (1992); however, we could not apply this transformation to the BD, because it is only calibrated for $H - K < 0.4$. Therefore, we calculated the $K' \rightarrow K$ transformations by integrating over DUSTY evolutionary model spectral energy distributions (SEDs) (Chabrier et al. 2000). We took the SED that most closely matched the color of the BD in our filters of interest (in this case, $H - K$). We used the same procedure for all color transformations for which empirical relations were not available. We calculated $K = 14.75\ mag$ for GSC 06214B. We then dereddened all GSC 06214B photometry, using the extinction value for the primary

$(A_V = 0.6)$ discussed in Section 3.1.2. We presumed the extinction toward the primary and secondary was the same, a nominally valid assumption, though counterexamples do exist (e.g. GG Tau, White & Ghez 2001). Figure 4 shows the color-color diagrams $H - L'/J - H$ and $H - M'/J - H$.

GSC 06214B was previously classified using $J/H/K$ spectra as a spectral type of L0±1 (Bowler et al. 2011). Its $J - H$ color is consistent with an L2010 spectral type of M9. The excesses at K, L', and M' compared to an L2010 M9 dwarf photosphere are 0.15 ± 0.05, 0.35 ± 0.07, and $0.4 \pm 0.3 \ mag$, respectively, accounting for photometric errors only. Fortuitously, the measured excesses are similar even if we use $A_V = 0$, because reddening moves the object up and right in color-color space parallel to the line connecting L2010 M9 and L0 spectral types. Therefore, our conclusions about the color excess for this object are independent of the extinction estimate, over the allowed range of extinction values.

3.1.4. 24 μm Flux

The GSC 06214 system was imaged with Spitzer/MIPS at 24 μm. The PSF is broader than the host-companion separation, so it is not possible to measure the primary and secondary objects' emission independently. However, the BD's photosphere does not contribute significantly at this wavelength. Whether based on a Rayleigh-Jeans extrapolation from short wavelength data or using DUSTY model SEDs, the BD's photospheric emission is expected to be less than 1% of the observed 24 μm flux.

We compared the MIPS photometry to the 24 μm flux predicted for the "A" component by an empirical polynomial relation between $V - K_S$ and 24 μm for main sequence stars (Urban et al. 2012). The 24 μm flux prediction is robust to order 0.01 mag between early B and early M spectral types. GSC 06214A is likely in the final stages of contraction onto the main sequence. However, the variation in $V - K_S$ color, and therefore in inferred 24 μm flux, between this object and a main sequence star, is less than the combined observational uncertainties at V, K_S, and 24 μm.

From this comparison, we find evidence of a 24 μm excess in the system. The observed system flux is $3.3 \pm 0.3 \ mJy$, while the predicted flux from "A" is $1.73 \pm 0.15 \ mJy$. This translates to an excess of $91 \pm 24\%$ above the expected photospheric emission from "A." The uncertainty is dominated by the low signal to noise of the 24 μm data. Our detection corroborates the 2σ excess at WISE 22 μm found by Bowler et al. (2011). Therefore, one or both members of the system must retain a warm excess.

3.1.5. Constraints on additional objects

No additional objects are detected in our observations. As discussed in Section 3.1.1, the candidate at $1''$ separation in M' is likely an artifact. In our collection of images, we could have detected additional companions of mass $\gtrsim 20 \ M_{Jup}$ at separations $\gtrsim 150 \ AU$ from the primary, with a limit of $\sim 10 - 12 \ M_{Jup}$ beyond 200 AU. Previous aperture masking and direct imaging work have placed deeper limits of $35/15/5 \ M_{Jup}$ at $10/150/300 \ AU$ from the primary (Kraus et al. 2008; Ireland et al. 2011). We would have resolved an equally bright binary com-

Table 3
1RXS 160929.1-210524 system properties and apparent photometry.

Property	1RXS 1609A	1RXS 1609B
Distance [pc] [a]	145±20	
Spectral type [b]	K7V	L4$^{+1}_{-2}$
Mass [b]	0.85$^{+0.20}_{-0.10}$ $M_\odot$	8$^{+4}_{-2}$ M_{Jup}
T_{eff} [b]	4060$^{+300}_{-200}$	1800$^{+200}_{-100}$
$log(L/L_\odot)$ [b]	-0.37±0.15	-3.55±0.2
Separation [$''$] [c]	2.15±0.03	
PA [°] [c]	28.3±0.4	
J	9.820±0.027 [d]	17.90±0.12 [b,e]
H	9.121±0.023 [d]	16.87±0.07 [b,e]
K	8.916±0.021 [d]	16.19±0.05 [b,e]
3.1 μm [c]	8.80±0.05	15.65±0.21
3.3 μm [c]	8.78±0.05	15.2±0.16
3.4 μm [g]	8.767±0.023	
L' [e,f]	8.73±0.05	14.8±0.3
4.5 μm [h]	8.80±0.01	
4.6 μm [g]	8.779±0.021	
8.0 μm [h]	8.735±0.005	
12 μm [g]	8.715±0.027	
24 μm [i]	8.43±0.01	

[a] Mean cluster distance (de Zeeuw et al. 1999; Preibisch et al. 2002).
[b] Lafrenière et al. (2008).
[c] This work.
[d] 2MASS $J/H/K_S$ survey (Skrutskie et al. 2006).
[e] MKO $J/H/K'/L'$.
[f] Lafrenière et al. (2010)
[g] System. WISE survey (Wright et al. 2010).
[h] System. Spitzer IRAC (Carpenter et al. 2006).
[i] System. Spitzer MIPS (Carpenter et al. 2009).

panion to "B" (i.e. "Bb") if it was > 20 AU projected separation from "B."

3.2. 1RXS 1609

3.2.1. Photometry and Astrometry

Figure 5 shows the final 1RXS 1609 narrowband images. We estimated the primary's 3.1 μm and 3.3 μm magnitudes to be 8.80 ± 0.05 and 8.78 ± 0.05, respectively. At 3.1 μm we found a contrast between "A" and "B" of 6.85 mag. The 5σ background sensitivity limit of 15.71 mag yielded $SNR = 5.3$ for the detection, thus $[3.1]_B = 15.65 \pm 0.21$. At 3.3 μm we found 6.4 mag contrast, a sensitivity limit of 16.14 mag, $SNR = 7.5$, and $[3.3]_B = 15.2 \pm 0.16$. (See Table 3).

We measured a separation of $2.15'' \pm 0.03''$ at $PA = 28.3° \pm 0.4°$, consistent with Lafrenière et al. (2010) at the 2σ level. These values represent the average of the astrometry calculated at 3.1 μm and 3.3 μm. Errors account for measurement uncertainties as well as our assumed calibration and distortion uncertainties (see Section 2.2.2).

3.2.2. Spectral Classification and Near-IR Colors

There is no extinction towards the 1RXS 1609 system (Carpenter et al. 2009). We transformed the K' companion photometry to yield $K = 15.99 \pm 0.1$, following the procedure described in Section 3.1.3. 1RXS 1609B is shown in the color-color diagrams in Figure 4.

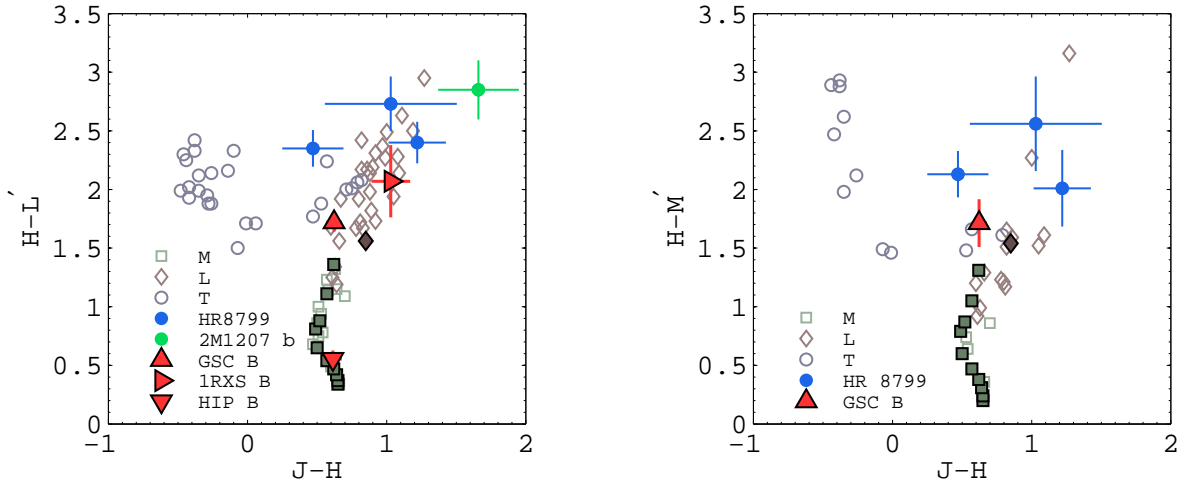Unfortunately, the L2010 sample does not extend past spectral type L0; we therefore compared 1RXS 1609B

Figure 4. $H - L'$ vs. $J - H$ *(left)* and $H - M'$ vs. $J - H$ *(right)* color-color diagrams of dereddened USco companions and comparison samples. Open green squares, brown diamonds, and gray circles: field M, L, and T dwarfs from Leggett et al. (2010); filled green squares and brown diamond: young M0–L0 dwarfs from L2010; filled blue circles: young planets HR 8799bcd (Currie et al. 2011; Marois et al. 2008a, 2010; Skemer et al. 2012; Galicher et al. 2011); filled green circle: young planet 2M 1207b (Mohanty et al. 2007).
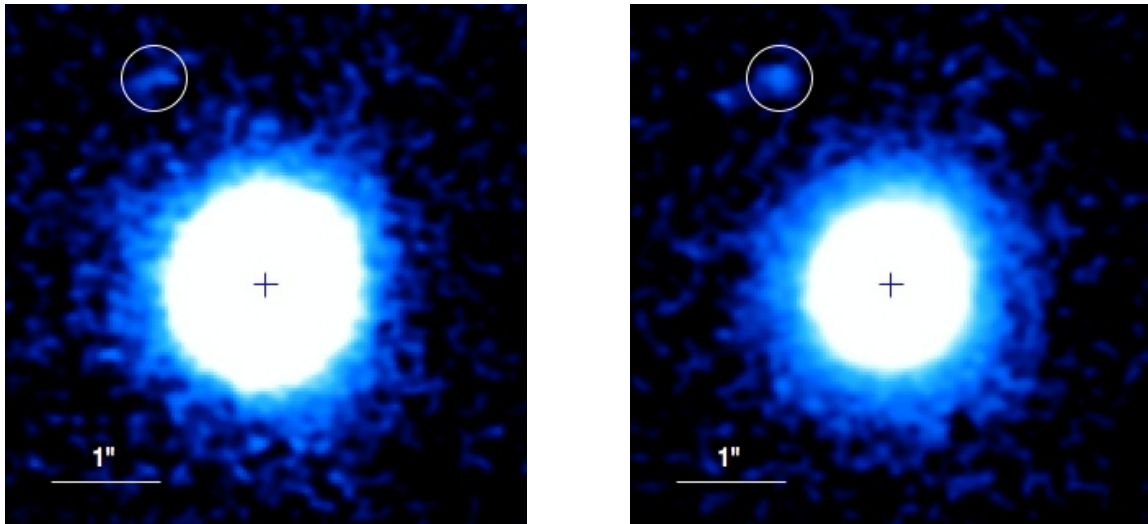
Figure 5. 1RXS 1609 Clio images. *Left:* 3.1 μm. *Right:* 3.3 μm. For display purposes, both are smoothed with a Gaussian kernel with FWHM=$1\lambda/D \sim 0.1''$. The companion, circled, is $2.2''$ to the NE.

broadband colors to DUSTY model SEDs with temperatures of $1700K$ and $1800K$. A surface gravity of $log(g) = 4.0$ is predicted by the DUSTY models for these effective temperatures at 5 Myr. We scaled the SEDs so their integrated J band flux matched the observed flux. Both SEDs provide an acceptable fit to the data (Figure 6), consistent with the Lafrenière et al. (2010) effective temperature estimate. Our new photometry confirms the lack of near-IR excess.

3.2.3. 24 μm Flux

Following the procedure used in Section 3.1.4, we find evidence for a moderate 24 μm excess in the system. The observed flux is 3.06 ± 0.04 mJy, and the predicted flux from "A" is 2.15 ± 0.07 mJy, an excess of $42 \pm 6\%$ above the expected stellar photospheric emission. The error is dominated by the uncertainty in the literature V magnitude. As with GSC 06214, the predicted contribution to the excess from the BD's photosphere is $< 1\%$. Neither "A" nor "B" exhibits a near-infrared excess, and

the components have not been resolved at wavelengths longer than L'. Thus, though we can detect the presence of a warm excess in the system, we cannot determine whether it is around the primary, BD, or both.

3.2.4. Constraints on additional objects

We do not detect any additional objects in the 1RXS 1609 system. Our background limit at 3.3 μm was 15.6 mag, or ~ 5 M_{Jup}, extending out to 500 AU. We do not improve upon previous detection limits of $8/1$ M_{Jup} at $50/450$ AU stellocentric distance (Lafrenière et al. 2010). We could have detected an equally luminous binary companion to "B" (i.e. "Bb") at a separation > 25 AU from "B."

3.3. HIP 78530

3.3.1. Photometry and Astrometry

Figure 7 shows the final L' image of HIP 78530, with the BD to the southeast. For the primary, we inferred
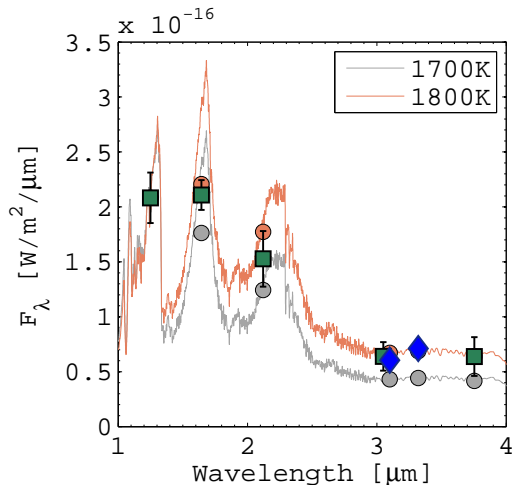
Figure 6. 1RXS 1609B photometry and DUSTY SED comparison with $A_V = 0$. The green squares are the literature photometry and the blue diamonds are this work. Spectra are DUSTY 1800K and 1700K model photospheres with $log(g) = 4.0$. The filled circles represent the integrated flux of each spectrum in that bandpass.

Table 4
HIP 78530 system properties and apparent photometry.

Property	HIP 78530A	HIP 78530B
Distance [pc] [a]		157 ± 13
Spectral type [b]	B9V	M8$\pm$1
Mass [b]	~ 2.5 $M_\odot$	23 ± 3 M_{Jup}
T_{eff} [K] [b]	~ 10500	2800 ± 200
$log(L/L_\odot)$ [b]	–	-2.55 ± 0.13
Separation [$''$] [c]		4.54 ± 0.09
PA [°] [c]		140.7 ± 1
J	6.928 ± 0.021 [d]	15.06 ± 0.05 [b]
H	6.946 ± 0.029 [d]	14.39 ± 0.04 [b]
K_s	6.903 ± 0.020 [d]	14.17 ± 0.04 [b]
3.4 μm [e]		6.842 ± 0.034
L' [c,f]	6.87 ± 0.05	13.80 ± 0.06
4.5 μm [g]		6.88 ± 0.01
4.6 μm [e]		6.890 ± 0.019
8.0 μm [g]		6.948 ± 0.008
12 μm [d]		6.924 ± 0.017
24 μm [h]		6.846 ± 0.01

[a] Hipparcos catalog (van Leeuwen 2007).
[b] Lafrenière et al. (2011).
[c] This work.
[d] 2MASS $J/H/K_S$ survey (Skrutskie et al. 2006).
[e] System. WISE survey (Wright et al. 2010).
[f] MKO L'.
[g] System. Spitzer IRAC (Carpenter et al. 2006).
[h] System. Spitzer MIPS (Carpenter et al. 2009).

$L'_A = 6.87 \pm 0.05$. HIP 78530B was detected at a contrast between "A" and "B" of 6.93 magnitudes (Table 4). The 5σ sensitivity limit was $L' = 16.21$, giving $SNR = 47$ and $L'_B = 13.80 \pm 0.06$. Our measured separation and PA are $4.54'' \pm 0.09''$ and $140.7° \pm 1°$, including plate scale and distortion uncertainties (see Section 2.2.1), consistent with previous observations.

3.3.2. *Spectral Classification and Near-IR Colors*

The extinction towards HIP 78530 is $A_V = 0.5$ (Carpenter et al. 2009), and we dereddened the photometry using this value. We calculated a K magnitude for the
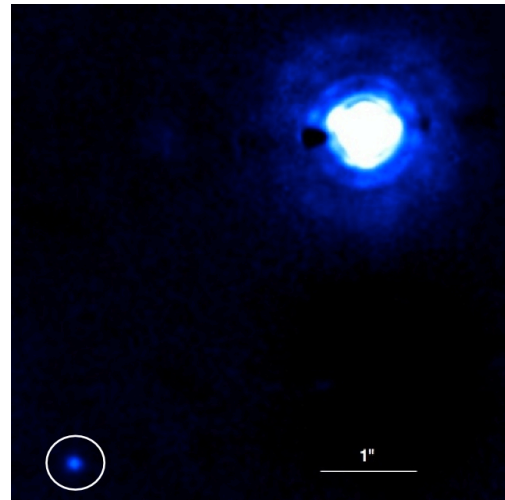

Figure 7. HIP 78530 LMIRCam L' image, smoothed for display purposes with a Gaussian kernel with FWHM=$1\lambda/D \sim 0.1''$. The companion, circled, is $4.5''$ to the SE.

BD of 14.12 ± 0.06 following the prescription described in Section 3.1.3.

We find the spectral types derived for HIP 78530B from broadband $1 - 4$ μm colors and from near-IR spectra are not consistent. HIP 78530B was classified using $J/H/K$ spectra as M8 ± 1 (Lafrenière et al. 2011), though the authors noted the object was ~ 0.2 mag too blue at K for this spectral type. We find that its $H - L'$ color is also ~ 0.5 mag too blue compared to an L2010 M8-type BD (Figure 4, left panel). There is a similar mismatch in both $H - K$ and $K - L'$ colors (Figure 8, left panel). With the addition of our new L' data, we find the object's J through L' colors are not consistent with an M8, but instead with an L2010 M3 ± 2. Intriguingly, the object's absolute magnitude is consistent with other USco M8-type BD (Luhman & Mamajek 2012) as shown in Figure 8 (right panel). We discuss the implications of this discrepancy further in Section 4.2. Regardless of whether we adopt spectral class M8 or M3, we find no evidence for K or L' excesses.

3.3.3. *24 μm Flux*

The observed and predicted fluxes for the HIP 78530 system are 13.10 ± 0.12 mJy and 12.0 ± 0.5 mJy. The excess is $9 \pm 4.5\%$. At 2σ, we do not consider it statistically significant. This, combined with a lack of $1 - 5$ μm excess around both "A" and "B," suggests that neither object retains a massive warm disk.

3.3.4. *Constraints on additional objects*

No additional objects are detected in our data. Figure 9 plots our new contrast and mass limits as a function of projected stellocentric distance; we adopt the Hipparcos system distance of 157 pc (van Leeuwen 2007). We reach a sensitivity of 20 M_{Jup} beyond 100 AU and $\lesssim 5$ M_{Jup} beyond 175 AU. In the east half of the system, our FOV extended to 800 AU, while on the west side, the FOV ended at ~ 200 AU. An equally luminous binary companion to "B" (i.e. "Bb") is ruled out at > 15 AU separation from "B."

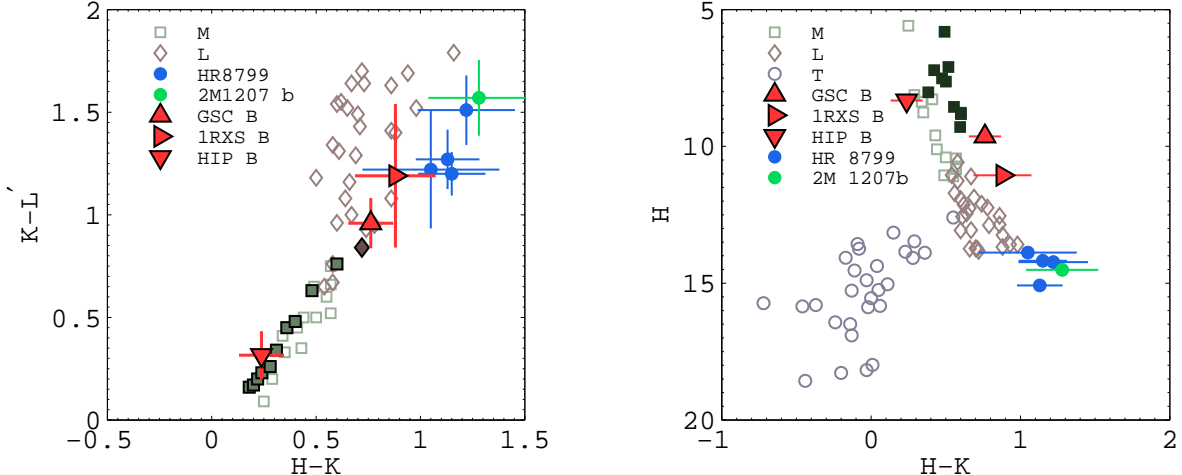### 4. DISCUSSION

Figure 8. $K - L'$ vs. $H - K$ color-color diagram *(left)* and H vs. $H - K$ color-magnitude diagram *(right)* of dereddened USco companions and comparison samples. Open green squares, brown diamonds, and gray circles: field M, L, and T dwarfs from Leggett et al. (2010); filled green squares and brown diamond: young M0–L0 dwarfs from L2010; black filled squares: diskless USco objects with spectral between M7–M8.5 (Luhman & Mamajek 2012); filled blue circles: young planets HR 8799bcde (Currie et al. 2011; Marois et al. 2008a, 2010; Skemer et al. 2012); filled green circle: young planet 2M 1207b (Mohanty et al. 2007).
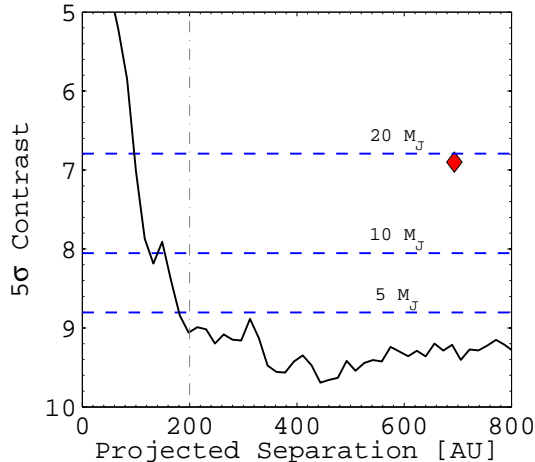
Figure 9. LMIRCam L' 5σ contrast curve for HIP 78530 (black line). Red diamond is HIP 78530B. Dashed lines are apparent magnitudes for objects of various masses according to 5 Myr DUSTY models. The dot-dashed line denotes the extent of the FOV on the west half of the system.

4.1. *GSC 06214B Disk Properties*

GSC 06214B was already known to exhibit an L' excess as well as Paβ emission, suggesting a circum(sub)stellar disk (Bowler et al. 2011). We wished to test this hypothesis using the full collection of $1 - 5$ μm and 24 μm photometry. The shape of the $1 - 5$ μm excess SED is strongly dependent on the temperature (location) of the inner edge of the disk. An accreting dust disk would likely be truncated at the dust sublimation temperature or by magnetic interactions near the corotation radius (Shu et al. 1994; Muzerolle et al. 2003), both of which are a few times the BD radius.

To estimate the location of the disk inner edge, we created simple model rings of blackbody grains at a single temperature. A disk with an inner edge at a temperature of 1550 K, the sublimation temperature of silicates, reproduced the shape of the observed J through M' excess. Decreasing the temperature to 1000 K under-produced

J, H, and K flux relative to the L' and M' flux. From this we conclude that hot dust must be present within several BD radii away from the BD's surface, consistent with what we expect for an actively accreting disk.

Adding additional weight to the disk hypothesis is the 24 μm excess. As described in Section 3.1.4, the GSC 06214 system has an unresolved 1.6 mJy excess at 24 μm. Luhman & Mamajek (2012) recently compiled $K_s - [24]$ and $[4.5] - [24]$ colors for other low-mass USco objects. The ratios of the 24 μm excess to the K and M' fluxes of GSC 06214B fall within the range that the authors derived for other disk-bearing late M-type objects in the association. Although the primary is shown to have Hα emission, presumably due to an accretion disk, the data are consistent with both the near- and mid-IR broadband excesses originating from a single, continuous disk around the BD.

4.2. *HIP 78530B Spectral Type and Membership*

As discussed in Section 3.3.2, HIP 78530B's broadband colors do not match the M8 spectral class indicated by the shape of its $J/H/K$ spectra. The L2010 young photosphere color calibration suggests it is an M3 $\pm$ 2 spectral type (Figures 4 and 8), and the observed colors also more closely match M3V colors than M8V colors (SPEX standards Gl 388 and LP 412-31, respectively). Using the temperature scale calibrated by Luhman et al. (2003), M3 corresponds to an effective temperature of $3300 - 3400$ K. The BCAH 5 Myr evolutionary models (Baraffe et al. 1998) predict a mass of $0.18 - 0.4$ $M_\odot$, depending on whether the 3350 K effective temperature, the $H - K$ color, or the $H - L'$ color is used. Regardless of the particular assumptions, these models place the object above the hydrogen burning limit (~ 75 M_J).

Conversely, the apparent magnitude of this object is consistent with other M8 brown dwarfs in Upper Sco (Figure 8) as well as the DUSTY and BCAH predictions for a $5 - 10$ Myr, 20 M_{Jup} BD. The 13 pc uncertainty in distance to HIP 78530A cannot account for the faintness of the object compared to other USco M3 BDs. New photometry at M' would help determine whether the object

is blue at all wavelengths or merely faint at K and L'.

Although the primary has a Hipparcos parallax which is consistent with the distance to USco, it is possible that "B" is a background object. In the discovery paper, Lafrenière et al. (2011) found agreement between the strength of gravity-sensitive NIR spectral features in HIP 78530B and those in another USco M8 BD. Additionally, the authors measured common proper motion at the 6σ level over a 2 year baseline. Unfortunately our astrometric calibration is not sufficiently precise to confirm or deny common proper motion. An additional epoch of observation would help to cement this object's status as a bound companion.

5. DISKS AS CONSTRAINTS ON SCATTERING EVENTS

The presence of an accreting disk around a low-mass companion at a wide separation from its primary star has the potential to limit the possible formation histories of the companion. To see why this is the case, we consider the fate of a gas disk orbiting a brown dwarf of mass M, which is in turn orbiting a star of mass M_*. An encounter or series of encounters with a perturber of mass $M_p > M$, also orbiting the primary star, can scatter the brown dwarf to wide separations, while typically leaving the more massive perturber on an orbit near the primary.

Each encounter truncates the disk at a distance, r, from the brown dwarf. This truncation distance is roughly the location where the tidal force during the encounter generates a velocity kick $\Delta v \sim (GM_p/b^2)(r/b)(2b/v_{\rm enc})$ equal to the escape velocity from the brown dwarf, $v_{\rm esc} = (2GM/r)^{1/2}$, where G is the gravitational constant, and b and $v_{\rm enc}$ are the distance of closest approach and the relative velocity of the two bodies during the encounter, respectively. We consider a fiducial encounter for which b is of order the Hill radius of the perturber, $b \sim R_{H,p} = a(M_p/3M_*)^{1/3}$ and $v_{\rm enc} = \Omega b$, is the relative velocity of two circular Keplerian orbits with semi-major axes that differ by b. Here, a is the distance from the host star at which the encounter occurs, and $\Omega = (GM_*/a^3)^{1/2}$ is the angular velocity of a circular orbit at that distance. These choices are intended to maximize the expected disk truncation during scattering, without invoking unusually close or slow encounters, which we expect to be rare. Note that arbitrarily extreme encounters are disallowed because the BD cannot be ejected from the system. Setting $\Delta v = v_{\rm esc}$ yields a truncation radius of $r \sim 0.5R_H$, where R_H is the brown dwarf's Hill radius. The disk truncation radius from scattering is thus predicted to be comparable to the radius generated merely by long-term tidal interactions with the host star, $\sim 0.4R_H$ (e.g. Martin & Lubow 2011). To solidify interpretation of future observations, we suggest that numerical simulations of scattering histories producing wide-separation BD companions should be mined to determine the typical properties of their most disruptive close encounters.

Although scattering does not significantly strip disk material from the BD, the disk can still be used to constrain the BD's scattering history. This is because the disk size, $\sim 0.4R_H$, is directly proportional to a, the semi-major axis at which the BD formed. We next estimate the range of formation locations which would produce disks large enough to survive for 5 Myr, the minimum age of USco.

Observations of protoplanetary disks at separations of tens of AU yield surface density profiles of order $\Sigma = 10^3$ g/cm^2 $(r/{\rm AU})^{-1}$ (Andrews et al. 2009), comparable to the minimum-mass solar nebula. Disks around brown dwarfs are likely less massive, so this profile places an upper limit on the disk lifetime. If such profiles extend inward to smaller separations from the BD, a typical disk contains a mass of $M_d \sim 7 \times 10^{-4} M_\odot (r/{\rm AU})$ within a radius r. The size of the inner clearing of an accreting disk is negligible, as we found in Section 4.1. Assuming that a typical low-mass brown dwarf has an accretion rate comparable to GSC 06214B, $\dot{M} = 2 \times 10^{-11} M_\odot/yr$ (Bowler et al. 2011), it would accrete at least $10^{-4} M_\odot$ of material over 5 Myr, the estimated mass interior to $r = 0.15$ AU. A higher accretion rate of $10^{-10} M_\odot/yr$ would process $5 \times 10^{-4} M_\odot$ over 5 Myr, equal to the estimated mass within $r = 0.7$ AU.

These estimates of the minimum disk size can be used to constrain the formation location of the BD. A truncation radius of $0.4a(M/3M_*)^{1/3}$ corresponds to $0.06a - 0.07a$ for our three BDs, using the masses listed in Tables 2, 3, and 4. We estimate that insufficient mass would remain in the current disk orbiting GSC 06214B if the brown dwarf were scattered outward by a perturber or perturbers from a stellocentric distance of $a \lesssim 2 - 10$ AU. Current limits on additional companions in the GSC 06214 system can rule out $35M_{Jup} \sim 2M_B$ objects beyond 10 AU stellocentric distance (Section 3.1.5), disfavoring, though note entirely ruling out, the scattering hypothesis. Limits on the minimum semi-major axis at formation of HIP 78530B and 1RXS 1609B, based on their lack of accretion signatures, are similar, presuming they had accretion rates similar to that of GSC 06214B. Additional objects more than twice as massive as the known BDs are ruled out beyond 35AU for 1RXS 1609 and beyond 75 AU for HIP 78530 (Lafrenière et al. (2010) and 3.3.4). These weaker constraints cannot be used to rule out a scattering origin for either object. Given our estimates, tighter observational constraints on the presence of possible perturbers, coupled with more detailed modeling of disk truncation during ejection by scattering will provide significant limits on the scattering histories of wide-separation, low-mass companions.

6. SUMMARY AND FUTURE WORK

We present a 3–5 μm LBT/MMT imaging study of three low-mass (ratio) companions to Upper Scorpius stars: GSC 06214B, 1RXS 1609B, and HIP 78530B. These three systems constitute some of the lowest mass-ratio ($q \sim 1\%$) non-planetary systems discovered to date. However, though the companions have similar separations and mass ratios, they probe two very different types of binary systems: GSC 06214 and 1RXS 1609 are K-type/L-type pairs, while HIP 78530 is a B-type/M-type pair. Combined with MIPS-24 μm photometry, we use our new high-resolution near/thermal IR data to identify evidence for broadband disk emission from small dust grains around both the companions and the primary stars. Our study yields the following major results:

- We confirm the presence of a circum(sub)stellar disk around the L0-type BD GSC 06214B. Furthermore, we find the best fit temperature of the disk inner edge is at the dust sublimation tempera-

ture, consistent with active accretion. A moderate 24 μm excess in the system is plausibly explained by the contribution from the BD's disk, although some material must still be present around the primary in order to explain its Hα emission. The existence of a disk around GSC 06214B suggests, but does not conclusively prove, it has not undergone a scattering event.

- We find evidence of a weak 24 μm excess in the 1RXS 1609 system, but the < 4 μm photometry of the primary and low-mass companion are consistent with purely photospheric emission. The 24 μm excess is unresolved, so we cannot determine whether "A," "B," or both host a warm disk.

- In contrast, we find no evidence of $1 - 4$ μm or 24 μm excesses in the HIP 78530 system. However, we find a discrepancy between the spectral types indicated by the $1 - 4$ μm broadband colors and by the $J/H/K$ spectra. Although the spectra and apparent magnitude are consistent with an USco M8-type BD, the broadband colors instead match a young M3-type low-mass star. Future work corroborating common proper motion in the system is necessary to decisively rule out the possibility that "B" is a background object. We present improved constraints on the presence of additional low-mass companions, ruling out equally luminous companions at projected separations from the primary > 100 AU and reaching a background limit of < 5 M_{Jup} beyond 175 AU.

Although our sample size is too small for robust statistics, the detection of a massive, hot disk in one of three low-mass companions is consistent with the disk fraction determined for single BDs in USco (Riaz et al. 2012; Scholz et al. 2007; Luhman & Mamajek 2012). Furthermore, though the range and relative importance of formation mechanisms for low-mass, widely separated companions remains unclear, this work does provide some constraints on the formation of our USco targets.

In particular, we corroborate the findings of Bowler et al. (2011), who identified a disk around GSC 06214B from accretion-driven Paβ emission. Our study further confirms that this disk is dusty, producing a strong broadband IR excess from grains near the dust sublimation radius, much like for many disks around stars in USco (Carpenter et al. 2006, 2009; Luhman & Mamajek 2012). The presence of a dusty, accreting disk around the BD, combined with the constraint that no object more than twice as massive as "B" exists beyond 10 AU stellocentric distance, casts doubt on whether this companion could have been formed via a planet-planet scattering event (i.e. as in Veras et al. 2009).

We do not detect a near-IR broadband excess around 1RXS 1609B. (The fact that the L4-type 1RXS 1609B does not have a hot disk, while the more massive L0-type GSC 06214B does, need not be contradictory; it is within the scatter in the inner disk dissipation timescale.) We do, however, find the system as a whole exhibits a 24 μm excess, presumably from warm dust. If some of this emission originates from a large disk surrounding the BD companion, then a scattering origin for this BD may also be disfavored.

Conversely, a lack of 24 μm excess around the more massive HIP 78530B does not necessarily imply a past scattering event, as depletion of warm dust from passive disk evolution alone is more rapid for intermediate-mass than for low-mass BDs (Luhman & Mamajek 2012).

Resolved observations with ALMA and/or NOMIC (the $8-13$ μm channel of LBTI) would be able to further constrain the disk properties of both the GSC 06214 primary and BD and could clarify whether the 1RXS 1609 system's warm 24 μm excess emission originates solely from material around the primary or around the low-mass companion as well. ALMA observations could in principle identify even colder dust emission from outer disk regions and provide a direct measurement of disk mass. They might also be used to differentiate between fully depleted disks and those with central clearings. A comparison of the incidence, masses, and morphologies derived in this way for disks around a larger sample of single and companion BDs might discriminate between in situ formation and scattering events. Finally, comparing cluster mass functions with age may identify a time-dependent low-mass BD population consistent with some fraction of low-mass BDs having a scattering origin.

REFERENCES

Andrews, S. M., Wilner, D. J., Hughes, a. M., Qi, C., & Dullemond, C. P. 2009, The Astrophysical Journal, 700, 1502

Baraffe, I., Chabrier, G., Allard, F., & Hauschildt, P. H. 1998, Astronomy & Astrophysics, 337, 403

Barman, T., Macintosh, B., Konopacky, Q., & Marois, C. 2011, The Astrophysical Journal Letters, 735, L39

Bate, M. R. 2000, Monthly Notices of the Royal Astronomical Society, 314, 33

Boss, A. P. 2011, The Astrophysical Journal, 731, 74

Bowler, B. P., Liu, M. C., Kraus, A. L., Mann, A. W., & Ireland, M. J. 2011, The Astrophysical Journal, 743, 148

Brusa, G., Miller, D. L., Kenworthy, M., Fisher, D., & Riccardi, A. 2004, Proceedings of SPIE, 5490, 23

Burgasser, A. J., Kirkpatrick, J. D., Reid, I. N., Brown, M. E., Miskey, C. L., & Gizis, J. E. 2003, The Astrophysical Journal, 586, 512

Canup, R., & Ward, W. 2002, The Astronomical Journal, 124, 3404

Cardelli, J. A., Clayton, G. C., & Mathis, J. S. 1989, The Astrophysical Journal, 345, 245

Carpenter, J. M., Mamajek, E. E., Hillenbrand, L. A., & Meyer, M. R. 2006, The Astrophysical Journal Letters, 651, L49

Carpenter, J. M., Mamajek, E. E., Hillenbrand, L. a., & Meyer, M. R. 2009, The Astrophysical Journal, 705, 1646

Carson, J., et al. 2013, The Astrophysical Journal Letters, 763, L32

Chabrier, G., Baraffe, I., Allard, F., & Hauschildt, P. 2000, The Astrophysical Journal, 542, 464

Chauvin, G., Lagrange, A., Dumas, C., Zuckerman, B., Mouillet, D., Song, I., Beuzit, J., & Lowrance, P. 2004, Astronomy & Astrophysics, 425, L29

Close, L. M., Siegler, N., Freed, M., & Biller, B. 2003, The Astrophysical Journal, 587, 407

Currie, T., Lada, C. J., Plavchan, P., Robitaille, T. P., Irwin, J., & Kenyon, S. J. 2009, The Astrophysical Journal, 698, 1

Currie, T., et al. 2011, The Astrophysical Journal, 729, 128

—. 2012, The Astrophysical Journal, 760, L32

Dawson, P., Scholz, A., Ray, T. P., Marsh, K. a., Wood, K., Natta, A., Padgett, D., & Ressler, M. E. 2013, Monthly Notices of the Royal Astronomical Society, 429, 903

de Zeeuw, P. T., Hoogerwerf, R., de Bruijne, J. H. J., Brown, A. G. A., & Blaauw, A. 1999, The Astronomical Journal, 117, 354

Diolaiti, E., Bendinelli, O., Bonaccini, D., Close, L. M., Currie, D. G., & Parmeggiani, G. 2000, Proceedings of SPIE, 4007, 879

Engelbracht, C. W., et al. 2007, Publications of the Astronomical Society of the Pacific, 119, 994

Esposito, S., et al. 2011, Proceedings of SPIE, 8149, 814902

Fischer, D. A., & Marcy, G. W. 1992, The Astrophysical Journal, 396, 178

Galicher, R., Marois, C., Macintosh, B., Barman, T., & Konopacky, Q. 2011, The Astrophysical Journal, 739, L41

Gordon, K., et al. 2005, Publications of the Astronomical Society of the Pacific, 117, 503

Hinz, P. M., Solheid, E., Durney, O., & Hoffmann, W. F. 2008, Proceedings of SPIE, 7013, 701339

Ireland, M. J., Kraus, A., Martinache, F., Law, N., & Hillenbrand, L. 2011, The Astrophysical Journal, 726, 113

Janson, M., Jayawardhana, R., Girard, J. H., Lafrenière, D., Bonavita, M., Gizis, J., & Brandeker, A. 2012a, The Astrophysical Journal, 758, L2

Janson, M., et al. 2012b, The Astrophysical Journal, 754, 44

Jensen, E. L. N., Mathieu, R. D., & Fuller, G. A. 1996, The Astrophysical Journal, 458, 312

Joergens, V. 2008, Astronomy & Astrophysics, 492, 545

Kalas, P., et al. 2008, Science, 322, 1345

Kratter, K. M., Murray-Clay, R. a., & Youdin, A. N. 2010, The Astrophysical Journal, 710, 1375

Kraus, A., Ireland, M., Hillenbrand, L., & Martinache, F. 2012, The Astrophysical Journal, 745, 19

Kraus, A. L., Ireland, M. J., Martinache, F., & Lloyd, J. P. 2008, The Astrophysical Journal, 679, 762

Lafrenière, D., Jayawardhana, R., Janson, M., Helling, C., Witte, S., & Hauschildt, P. 2011, The Astrophysical Journal, 730, 42

Lafrenière, D., Jayawardhana, R., & Van Kerkwijk, M. 2008, The Astrophysical Journal Letters, 689, L153

Lafrenière, D., Jayawardhana, R., & Van Kerkwijk, M. H. 2010, The Astrophysical Journal, 719, 497

Lagrange, A.-M., et al. 2010, Science, 329, 57

Leggett, S. K., Burningham, B., & Saumon, D. 2010, The Astrophysical Journal, 710, 1627

Leggett, S. K., et al. 2006, Monthly Notices of the Royal Astronomical Society, 373, 781

Lloyd-Hart, M. 2000, Publications of the Astronomical Society of the Pacific, 112, 264

Luhman, K. L., Allen, P. R., Espaillat, C., Hartmann, L., & Calvet, N. 2010, The Astrophysical Journal Supplement Series, 186, 111

Luhman, K. L., Hernández, J., Downes, J. J., Hartmann, L., & Briceño, C. 2008, The Astrophysical Journal, 688, 362

Luhman, K. L., & Mamajek, E. E. 2012, The Astrophysical Journal, 758, 31

Luhman, K. L., Stauffer, J. R., Muench, A. A., Rieke, G. H., Lada, E. A., Bouvier, J., & Lada, C. J. 2003, The Astrophysical Journal, 593, 1093

Luhman, K. L., et al. 2006, The Astrophysical Journal, 649, 894

Lunine, J. I., & Stevenson, D. J. 1982, Icarus, 52, 14

Marcy, G. W., & Butler, R. P. 2000, Publications of the Astronomical Society of the Pacific, 112, 137

Marois, C., Lafrenière, D., Doyon, R., Macintosh, B., & Nadeau, D. 2006, The Astrophysical Journal, 641, 556

Marois, C., Lafreniere, D., Macintosh, B., & Doyon, R. 2008a, The Astrophysical Journal, 673, 647

Marois, C., Macintosh, B., Barman, T., Zuckerman, B., Song, I., Patience, J., Lafrenière, D., & Doyon, R. 2008b, Science, 322, 1348

Marois, C., Zuckerman, B., Konopacky, Q. M., Macintosh, B., & Barman, T. 2010, Nature, 468, 1080

Martin, R. G., & Lubow, S. H. 2011, Monthly Notices of the Royal Astronomical Society, 413, 1447

Metchev, S. A., & Hillenbrand, L. A. 2006, The Astrophysical Journal, 651, 1166

Mohanty, S., Jayawardhana, R., Huelamo, N., & Mamajek, E. E. 2007, The Astrophysical Journal, 657, 1064

Monin, J.-L., et al. 2010, Astronomy and Astrophysics, 515, A91

Muzerolle, J., Hillenbrand, L. A., Calvet, N., Briceño, C., & Hartmann, L. 2003, The Astrophysical Journal, 592, 266

Pascucci, I., Apai, D., HardegreeUllman, E. E., Kim, J. S., Meyer, M. R., & Bouwman, J. 2008, The Astrophysical Journal, 673, 477

Pecaut, M. J., Mamajek, E. E., & Bubar, E. J. 2012, The Astrophysical Journal, 746, 154

Pickles, A. J. 1998, Publications of the Astronomical Society of the Pacific, 110, 863

Preibisch, T., Brown, A. G. A., Bridges, T., Guenther, E., & Zinnecker, H. 2002, The Astronomical Journal, 124, 404

Raghavan, D., et al. 2010, The Astrophysical Journal Supplement Series, 190, 1

Reggiani, M. M., & Meyer, M. R. 2011, The Astrophysical Journal, 738, 60

Riaz, B., Lodieu, N., & Gizis, J. E. 2009, The Astrophysical Journal, 705, 1173

Riaz, B., Lodieu, N., Goodwin, S., Stamatellos, D., & Thompson, M. 2012, Monthly Notices of the Royal Astronomical Society, 420, 2497

Rodigas, T. J., et al. 2012, The Astrophysical Journal, 752, 57

Scholz, A., Jayawardhana, R., & Wood, K. 2007, The Astrophysical Journal, 660, 1517

Shu, F., Najita, J., Ostriker, E., Wilkin, F., Ruden, S., & Lizano, S. 1994, The Astrophysical Journal, 429, 781

Sivanandam, S. 2006, Proceedings of SPIE, 6269, 62690U

Skemer, A. J., Close, L. M., Szcs, L., Apai, D., Pascucci, I., & Biller, B. A. 2011, The Astrophysical Journal, 732, 107

Skemer, A. J., et al. 2012, The Astrophysical Journal, 753, 14

Skrutskie, M. F., Jones, T., Hinz, P., Garnavich, P., Wilson, J., Nelson, M., & Solheid, E. 2010, Proceedings of SPIE, 7735, 77353H

Skrutskie, M. F., et al. 2006, The Astronomical Journal, 131, 1163

Song, I., Zuckerman, B., & Bessell, M. S. 2012, The Astronomical Journal, 144, 8

Spiegel, D. S., Burrows, A., & Milsom, J. a. 2011, The Astrophysical Journal, 727, 57

Tuthill, P. G., Monnier, J. D., & Danchi, W. C. 2001, Nature, 409, 1012

Urban, L. E., Rieke, G., Su, K., & Trilling, D. E. 2012, The Astrophysical Journal, 750, 98

van Leeuwen, F. 2007, Astronomy & Astrophysics, 474, 653

Veras, D., Crepp, J. R., & Ford, E. B. 2009, The Astrophysical Journal, 696, 1600

Wainscoat, R. J., & Cowie, L. L. 1992, The Astronomical Journal, 103, 332

White, R. J., & Ghez, A. M. 2001, The Astrophysical Journal,
    556, 265

Wright, E. L., et al. 2010, The Astronomical Journal, 140, 1868